High-performance transparent conducting oxides through small-polaron transport

Guillaume Brunin, Gian-Marco Rignanese, and Geoffroy Hautier*
UCLouvain, Institut de la Matière Condensée et des Nanosciences (IMCN), Chemin des Étoiles 8, Louvain-la-Neuve 1348, Belgium

(Received 17 December 2018; revised manuscript received 22 March 2019; published 13 June 2019)

Transparent conducting oxides (TCOs) are essential to many technologies including solar cells and transparent electronics. The search for high-performance *n*- or *p*-type TCOs has mainly focused on materials offering transport through band carriers instead of small polarons. In this work, we break this paradigm and demonstrate using well-known physical models that, in certain circumstances, TCOs exhibiting transport by small polarons offer a better combination of transparency and conductivity than materials conducting through band transport. We link this surprising finding to the fundamentally different physics of optical absorption for band and polaronic carriers. Our work rationalizes the good performances of recently emerging small-polaronic Cr-based *p*-type TCOs such as Sr-doped $LaCrO_3$ and outlines design principles for the development of high-performance TCOs based on transport by small polarons. This opens new avenues for the discovery of high-performance TCOs especially *p*-type.

DOI: 10.1103/PhysRevMaterials.3.064602

I. INTRODUCTION

Transparent conducting oxides (TCOs) are exceptional materials combining the antagonistic properties of optical transparency and electrical conductivity [1,2]. The transparency of TCOs is usually achieved using wide optical band gap oxides (direct band gap $E_g > 3$ eV) and they are made highly conductive by the introduction of excess electrons (*n*-type) or holes (*p*-type) through intrinsic or extrinsic doping. Introducing these carriers can also, in some cases, improve the transparency of a material through the Moss-Burstein effect [3–6]. High-performance TCOs are essential to many modern technologies including solar cells, optoelectronic devices, touch screens and light emitting diodes [2,7,8]. The best *n*-type TCOs, based on doped In_2O_3, ZnO or SnO_2, show conductivities on the order of 10^4 S cm^{-1} and transmittances well above 80% [7,9–12]. On the other hand, *p*-type TCOs such as $ZnRh_2O_4$, $CuAlO_2$, and $SrCu_2O_2$ show much poorer performances. Their conductivities reach at most 10 S cm^{-1} for transparencies between 50% and 80% (for films of a few hundred nm thicknesses) [8,11,13]. This lack of high-performance *p*-type TCOs limits many applications in transparent electronics or new solar cell architectures [11].

Very recently, Cr-based oxides have shown attractive performances as *p*-type TCOs. Materials such as Cu-deficient $CuCrO_2$, Mg-doped Cr_2O_3 and more recently Sr-doped $LaCrO_3$ have shown among the best transparencies and conductivities for *p*-type oxides [14–19]. These Cr-based oxides exhibit a thermally activated mobility because charge transport occurs through small-polaron hopping. A small polaron consists of a charge carrier localized on a single atomic site due to the interactions with the surrounding ions. Small-polaron transport has usually been considered detrimental for TCO applications [2,11,20,21]. Indeed, the low mobilities of small polarons ($\mu \ll 1$ cm^{2}V^{-1}s^{-1}) compared to band carriers ($\mu \sim 0.1$–100 cm^2 V^{-1} s^{-1}) [22] are believed to prevent them to achieve high performances as TCOs. And even for applications in which conductivity (and not mobility) is the most important property, this low mobility needs to be counterbalanced by a higher carrier concentration which is traditionally correlated with the degradation of transparency [23].

These considerations have led the TCO community to advocate against the use of materials based on small-polaron transport. Naturally, this affected the search and design of new TCOs (including those computationally driven) with the avoidance of small-polaron formation often put forward as a criteria for a high-performance TCO [24]. The apparent contradiction between this criteria and the encouraging performances of Cr-based oxides has not been addressed so far in the literature. A clear rationalization of the true inconvenients and potentially overlooked benefits of TCOs based on small-polaron transport is therefore greatly needed.

Here, we use well-established physical models describing how transparency and conductivity vary with materials parameters (effective mass, carrier concentration,...) to compare the performances of ideal band and small-polaron TCOs. We show that TCOs relying on small-polaron transport (SP-TCOs) can outperform those relying on band transport (B-TCOs) especially when the latter exhibit a high effective mass (which is often the case for *p*-type oxides). The physical origin of this surprising result lies in the very different change of the optical absorption of B- and SP-TCOs as the carrier concentration increases. While B-TCOs see their optical transparency drop when high carrier concentrations are reached, SP-TCOs can remain highly transparent. Our results rationalize the good performances of Cr-based *p*-type polaronic oxides and motivate the TCO community to revise its avoidance for small-polaron materials. We also provide a series of design principles for the search of novel SP-TCOs.

*geoffroy.hautier@uclouvain.be

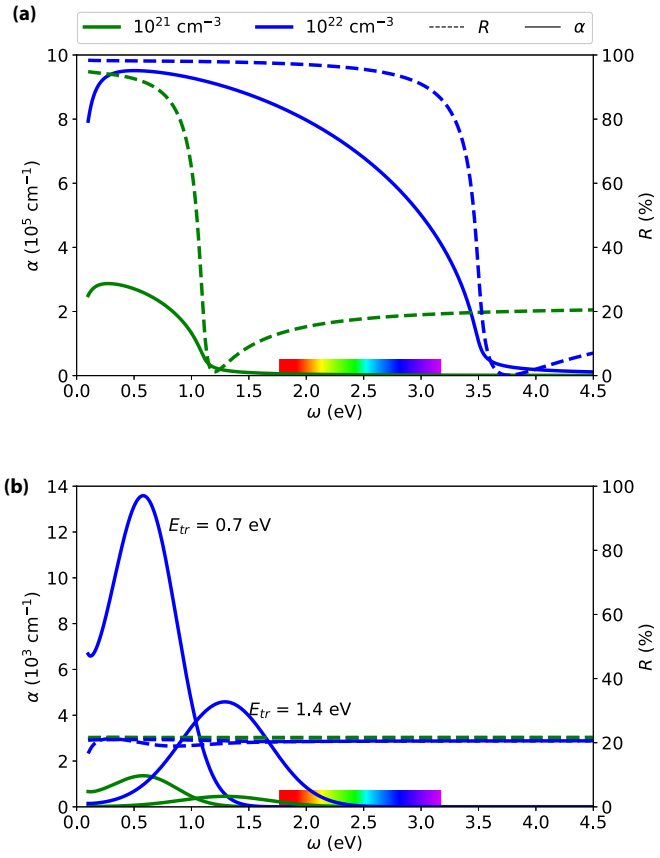

FIG. 1. Absorption coefficient α and reflectivity R for (a) B-TCOs with an effective mass $m^* = 0.15m_0$ and mobility $\mu = 90$ cm^2 V^{-1} s^{-1} and (b) SP-TCOs for two transition energies. Different carrier concentrations are shown: 10^{21} (in green) and 10^{22} cm^{-3} (in blue).

This opens an entirely new avenue towards the search and development of high-performance TCOs expecially p-type.

II. RESULTS

A. Comparison of performances for B- and SP-TCOs

The optical response of highly doped B-TCOs typically follows the Drude model which assumes an electron gas in a potential imposed by the nuclei. Figure 1(a) plots the reflectivity R and absorption coefficient α as functions of the energy ω of the light at different doping levels and for different material parameters (effective mass, mobilities) for the Drude model (see Secs. 1 and 2 for the full derivation in Ref. [25]). Below a certain threshold for the energy of the light, both the reflectivity R and the absorption coefficient α are large due to collective oscillations of the carrier gas. In this regime, the highly doped B-TCO behaves as a metal. The threshold in energy below which collective oscillations of the carriers happen corresponds to the so-called plasma frequency ω_p:

$$\omega_p^2 = \frac{Ne^2}{\varepsilon_r \varepsilon_0 m^*} \tag{1}$$

where N is the carrier concentration, e is the elementary charge, ε_r is the high-frequency limit of the real part of the dielectric function, ε_0 is the vacuum permittivity and m^* is the effective mass of the band carriers. When the carrier concentration in a B-TCO increases, the plasma frequency shifts towards higher energies and from the infrared to the visible spectrum. If the carrier concentration is too large, most visible light is reflected by the material while the rest is absorbed. This is clearly illustrated in Fig. 1(a) where a material transparent in the visible spectrum at 10^{21} cm^{-3} (in green) reflects and absorbs most of the visible light when doped to 10^{22} cm^{-3} (in blue). This phenomenon sets a limit to the doping level and therefore to the conductivity reachable in a B-TCO. As a result, a compromise needs to be found between maximizing the conductivity and the transmittance [23]. The transparency-conductivity compromise can be directly probed by plotting transmittance versus the sheet conductivity (i.e., the product of the conductivity and the thickness t of the material) [26]. Figure 2 reports the transmittance versus the sheet conductivity for B-TCOs with different materials properties: in green for low effective mass/high mobility (using the best values for n-type B-TCOs [1,11]) and in purple for high effective mass/low mobility (adopting typical good values for p-type B-TCOs [8,11]) materials. We have also considered other typical n-type TCOs parameters (mobility $\mu = 50$ cm^2 V^{-1} s^{-1} and effective mass $m^* = 0.3m_0$ [1]), and the transmittance versus sheet conductivity curve is similar to the one corresponding to the best parameters (leading to a larger mobility). The differences between the two are that (i) a larger carrier concentration is required when the mobility is lower to reach the same sheet conductivity, and (ii) the larger effective mass decreases the plasma frequency, allowing for larger carrier concentrations before the loss of transmittance. Solid lines in Fig. 2 indicate carrier concentrations lower than 10^{22} cm^{-3} while higher carrier concentrations are shown by

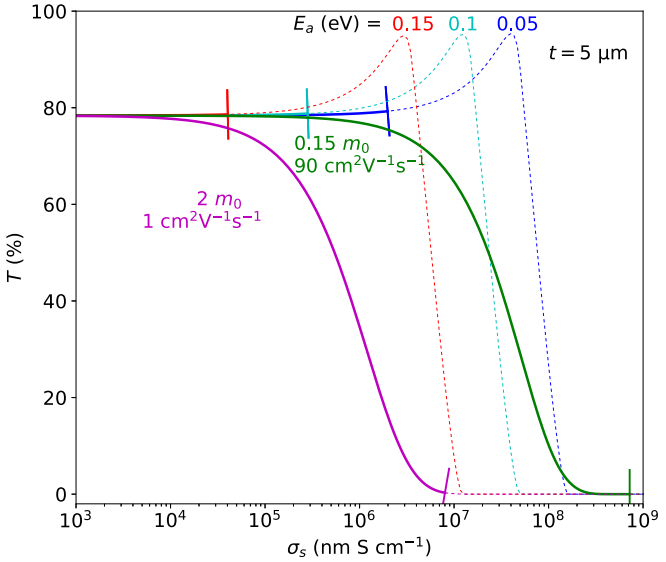

FIG. 2. Average transmittance T of visible light vs sheet conductivity σ_s for low effective mass/high mobility (green) and high effective mass/low mobility (purple) B-TCOs, and SP-TCOs (blue, cyan, and red) with various transport activation energies E_a. We used a thickness $t = 5$ μm. Solid (respectively, dashed) lines correspond to carrier concentrations lower (respectively, higher) than 10^{22} cm^{-3}.

dashed lines (as it is unlikely that higher carrier concentrations could be reached). For both low and high effective mass materials, increasing the sheet conductivity through higher carrier concentration leads at some point to a strong degradation of the transmittance. This degradation comes directly from the movement of the plasma edge towards higher frequencies. The low and high effective mass materials behave quantitatively differently: a higher sheet conductivity and transmittance can be reached for high-mobility materials. Hence, justifying the interest for high mobility/low effective mass TCOs as they offer larger transmittance and sheet conductivity when band transport is involved [11].

The optical response of SP-TCOs is extremely different from the one of B-TCOs. In the former, the carriers are trapped and cannot oscillate collectively. Optical transitions (additionally to the band gap interband transitions) are however present because of the small polarons. These can be excited to either a delocalized (free) state or to a small-polaron state at an adjacent site (see Ref. [25], Sec. 3). The physics of these processes has been studied and the absorption coefficient of a material containing small polarons is given by [27]

$$\alpha(\omega) = K_1 \frac{N}{\omega} \exp\left(\frac{-(E_{\text{tr}} - \hbar\omega)^2}{\Delta^2}\right) \tag{2}$$

with N the small-polaron concentration, E_{tr} the energy of the small-polaron transition, ω the frequency of the incoming light and K_1 a constant defined in Ref. [25], Sec. 3. This constant depends on the phonon and electronic properties as well as on the structure of the material but it is not expected to change significantly. Furthermore, it is only a prefactor to the dominant exponential term. Δ is the phonon broadening of the ground state. The absorption coefficient of an SP-TCO is plotted in Fig. 1(b) for two arbitrary transition energies (0.7 and 1.4 eV) and for different small-polaron concentrations (in green and blue). This figure also reports the reflectivity of SP-TCOs (see Ref. [25], Sec. 3). The latter is dominated by the polarization of ion cores which leads to a constant reflectivity in the whole range and is characterized by ε_r. The effect of small polarons, which leads to deviations with respect to this constant and depends on their transition energy and their concentration, is not significant for visible transparency. The curves corresponding to a large set of transition energies and concentrations are available in Ref. [25], Figs. 4–8.

Figure 1(b) shows that as the small-polaron concentration increases, only the absorption peak height is modified and not its position. This behavior is remarkably different from the one of B-TCOs in which the absorption edge shifts to higher energies when the carrier concentration increases, as can be seen in Fig. 1(a). If the small-polaron transition energy is small enough, the absorption peak is not significant in the visible spectrum and the SP-TCO remains transparent even when very high carrier concentrations are reached (10^{22} cm^{-3}). It has been experimentally observed in different SP-materials that the small-polaron regime holds even at very large carrier concentrations [14,16,28]. This indicates that the SP models that we use here can still be valid even for such large concentrations.

The physics of the transport in SP-TCOs is also very different from B-TCOs. The mobility μ of small polarons is thermally activated through an activation energy E_a needed for the polaron to hop from site to site [29]:

$$\mu = \frac{K_2}{k_B T} \exp\left(\frac{-E_a}{k_B T}\right) \tag{3}$$

with T the temperature, k_B the Boltzmann constant and K_2 a constant defined in Ref. [25], Sec. 3. This constant also depends on the phonon properties and on the structure of the material but it is not expected to change significantly, as compared to the exponential factor. The mobility directly impacts the conductivity and is much lower than 1 cm^2 V^{-1} s^{-1} when small polarons are involved. As we did for B-TCOs, we can combine the conductivity of small polarons with their optical response and analyze how the transmittance of a polaronic thin film changes with sheet conductivity. For SP-TCOs, there are two main parameters: the transition energy (E_{tr}), which determines the optical properties and the activation energy (E_a) which sets the electrical properties. In the commonly used Marcus theory these two quantities are actually linked through $E_a = \frac{E_{\text{tr}}}{4}$ [28,30]. For the sake of simplicity, we assume this relationship also holds here. SP-TCOs optical and electrical properties are thus controlled by only one parameter. Though there can be deviations from this relation due to interactions between small polarons in the material, the general conclusions are not affected by this assumption (as shown in Ref. [25], Fig. 9). Moreover, there are SP materials (e.g., $LaCrO_3$) having very large SP concentration ($>10^{21}$ cm^{-3}) that are still very well represented by this simple model.

In Fig. 2, next to the results for B-TCOs (purple and green), we plot the transmittance versus sheet conductivity for SP-TCOs with activation energies between 0.05 and 0.15 eV (in red, cyan and blue). Solid lines indicate carrier concentrations lower than 10^{22} cm^{-3} while higher carrier concentrations are shown by dashed lines (as it is unlikely that higher carrier concentrations could be reached). The transmittance dependence on the sheet conductivity for SP-TCOs is very different from the one for B-TCOs (purple and green). For SP-TCOs, the sheet conductivity can be enhanced by increasing the carrier concentration without degrading the transmittance up to concentrations as large as 10^{22} cm^{-3}. This directly originates from the very different physics of light absorption in SP- and B-TCOs, especially from the absence of plasma edge movement in the former.

From Fig. 2, we can already observe that the SP-TCOs can offer attractive combined values of transparency and conductivity. However, the performances of TCOs are more easily compared using a figure of merit (FoM) which provides one number per material aggregating its optical and electrical responses [26]. Several FoMs exist and we choose the one suggested by Haacke as it is one of the most widely used [31–34]. It is defined by $T^q\sigma_s$ with T the transmittance, σ_s the sheet conductivity and q an arbitrary exponent usually set to 10 in the literature [1,11,33,35]. Figure 3 plots the FoM versus thickness for the low and high effective mass B-TCOs (green and purple, respectively) and SP-TCOs with different activation energies (blue, cyan and red). The dotted and solid lines indicate different doping levels (10^{21} and 10^{22} cm^{-3}), and the shaded zones between them correspond to intermediate doping levels between these extremes. For each B-TCO, an optimal thickness maximizes the FoM [1]. The

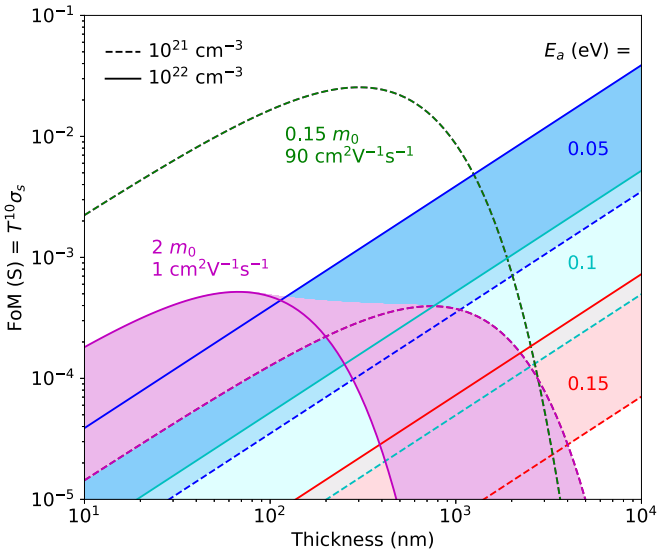

FIG. 3. Haacke figure of merit (FoM) vs material thickness for typical *n*-type (green) and *p*-type (purple) B-TCOs and SP-TCOs (blue, cyan and red) with various transport activation energies E_a. Dashed (respectively, solid) lines correspond to a carrier concentration of 10^{21} (respectively, 10^{22}) cm^{-3}. Concentrations between these two bounds are represented by colored zones.

high and low effective mass B-TCOs show similar behavior of the FoM versus thickness with optimal thicknesses from 100 nm to 1 μm and maximal FoMs respectively of 5×10^{-3} and 3×10^{-2} S. This explains the small thicknesses currently used in applications [1]. On the other hand, SP-TCOs (blue, cyan, and red) do not show an optimal thickness. As a result they can reach a similar level of FoM (3×10^{-2} S) as low effective mass/high mobility B-TCOs (in green), when they combine a very low activation energy (0.05 eV) with high carrier concentrations (10^{22} cm^{-3}), and if they are thick enough (around 10 μm). What is even more remarkable is that the SP-TCOs outperform by at least one order of magnitude in FoM the high effective mass/low mobility B-TCOs. At a thickness of 5 μm, SP-TCOs with an activation energy of at most 0.1 eV and a doping between 10^{21} and 10^{22} cm^{-3} will show larger FoM than low mobility B-TCOs of optimal thickness (100 nm–1 μm). To put it simply, an SP-TCO with adequate material properties (high doping level and low activation energy) will perform better than a lousy (low mobility/high effective mass) B-TCO. This conclusion is exacerbated in applications where transparency in the infrared is key (e.g., solar cells) [36–38]. Indeed, it is the plasma edge that is detrimental to IR transparency of highly doped B-TCOs and, in contrast, SP-TCOs with their absence of plasma edge offer excellent performances in the IR (see Ref. [25], Sec. 4). We should stress that a thickness on the order of the micrometer is compatible with various applications such as solar cells [39–42], making SP-TCOs very attractive. For applications requiring thinner films (∼100 nm), either B-TCOs or SP-TCOs with both a very low activation energy (0.05 eV) and a high dopability (10^{22} cm^{-3}) should be used as they offer similar performances (see Fig. 3).

The outperformance of low effective mass B-TCOs by SP-TCOs is especially relevant for *p*-type TCOs. Indeed, *n*-type B-TCOs are currently available with very low effective masses and high mobilities. Materials such as In_2O_3, ZnO or SnO_2 are well represented by the low effective mass green curve in Figs. 2 and 3. In this case, there is no strong incentive to favor small-polaron transport. However, the situation for *p*-type TCOs is drastically different with no high mobility/low effective mass *p*-type B-TCO available. In fact, the oxygen *p* character of the valence band in typical oxides is a major obstacle to the development of low effective mass *p*-type oxides. Data mining of large electronic structure databases have shown that it is extremely rare for a *p*-type transparent oxide to provide effective masses as low as current *n*-type TCOs [8,43]. Keeping in mind this tendency for large effective masses in *p*-type oxides, our analysis justifies the search for new high-performance *p*-type TCOs to turn to SP-TCOs.

B. New design route for *p*-type TCOs and the case of Sr-doped $LaCrO_3$

We have outlined the general principle that SP-TCOs can outperform high effective mass/low mobility transparent oxides. However, as for B-TCOs, there are certain material properties that are required to lead to a high-performance SP-TCO. Our analysis can be directly used to outline a series of materials design principles, helping the discovery of novel efficient SP-TCOs. The first requirement, which is already present for B-TCOs, is a large band gap (ideally >3 eV). Next, the SP-TCO needs to present excitation energies not affecting the visible transparency. Typically, polaronic transition energies lower than 1.2 eV are required. It is also critical to reach decent mobilities with a reasonably low activation energy [44]. Our analysis indicates that polaron activation energies from 0.15 eV to 0.05 eV are required. Finally, high dopability is even more important than in B-TCOs as the lower mobility needs to be compensated by higher carrier concentrations (typically 10^{21} to 10^{22} cm^{-3}). We should note that not only the dopant solubility should be high but that dopants should not introduce defects in the gap as they would lead to unwanted absorption. Our analysis using Haacke's FoM also stresses that such an ideal material would require to be deposited at thicknesses above the micrometer to maximize performances.

Cr-based oxides such as Cr_2O_3 and $CuCrO_2$ have been shown to involve small-polaron transport and decent TCO properties [16–19]. The material with the highest reported performances is Sr-doped $LaCrO_3$ and we will use our analysis to rationalize its performances [14,15]. We perform this comparison through a combination of previously reported experimental data on Sr-doped $LaCrO_3$ as well as our own first-principles computations. Details are presented in Ref. [25], Sec. 6. We computed from first principles a transition energy ranging between 0.56 and 0.79 eV in very good agreement with the experimental absorption peak observed by Zhang *et al.* at 0.7–0.8 eV [14]. Our computations assign this peak to the transition from the small-polaron state to the delocalized state. The computed activation energies for the hopping mechanism are ∼0.1 eV. The full data and the energy curves of the holes transfers are presented in Ref. [25], Sec. 6. The values are in good agreement with other theoretical

work and experimental transport measurements [15]. Our computed energy of mixing for Sr in $LaCrO_3$ are close to zero indicating that entropy will easily favor the mixing of Sr in the oxide (see Ref. [25], Sec. 6). Moreover, no defect states are introduced within the gap when Sr is incorporated in $LaCrO_3$.

$LaCrO_3$ appears to show all the design principles outlined previously and this rationalizes its good performances. However, the experimental Haacke's FoM of the best Sr-$LaCrO_3$ material lies several orders of magnitude lower than a perfect SP-TCO with the same activation energy (0.1 eV) and doping level (3.4×10^{21} cm^{-3}) [14]. The reason for this discrepancy comes from the band gap of $LaCrO_3$. Its experimental value is 2.8 eV [14,45,46] while our analysis assumes a material with a band gap higher than 3 eV. $LaCrO_3$ will thus absorb in the end of the visible spectrum. Moreover, as Sr is inserted in the material, our computations show that the band gap shrinks and the transmittance drops (see Ref. [25], Sec. 6) in agreement with the experimental observations [14]. This analysis indicates that alternative materials to $LaCrO_3$ keeping the low activation energy for polaron hopping with slightly larger band gaps could lead to substantial improvement in terms of *p*-type TCOs performances.

Li-doped NiO is another example of *p*-type SP-TCO [47]. The NiO thin films darken as the hole concentration increases. There are different possible reasons for this. First, as suggested by Ref. [48], there might be a shrinkage of the band gap, leading to an increase of the absorption coefficient, like in the case of $LaCrO_3$. As suggested in Ref. [49], intrinsic defect states might also increase the absorption coefficient. Finally, as is suggested by Ref. [47], there could be optical transitions between the small-polaron hole state and the O $2p^6$-Ni $3d$ states in the valence band at an energy between 1.4 and 3 eV. In any of these cases, Li-doped NiO does not fulfill the requirements to be an efficient small-polaron TCO.

Using well-known physical relations linking optical absorption and conductivity to material properties, we have shown that the transparency-conductivity compromise emerging from band carriers in B-TCOs does not exist when the transport is carried by small polarons. This important difference is linked to the absence of band carriers plasma absorption and reflection when the carriers are trapped and form small polarons. Our quantitative analysis of sheet conductivity versus transparency for TCOs exhibiting small-polaron or band-carrier transport shows that, in certain situations, SP-TCOs can outperform B-TCOs. This is especially the case when band carriers have large effective masses such as in typical *p*-type oxides. This result is surprising in view of the avoidance for small-polaron transport in the TCO field but rationalizes the recent emergence of relatively high-performance Cr-containing *p*-type TCOs (e.g., $LaCrO_3$). Our analysis leads to the outline of a series of materials design principles to develop high-performance SP-TCOs. These design principles include a low activation energy for hopping (<0.15 eV) and high small-polaron concentrations (i.e., needing high dopant solubility) without defect states within the gap. We hope our analysis will motivate both experimental and computational searches for polaronic materials that could lead to very high-performance TCOs especially *p*-type.

III. METHODS

A. Optical absorption and conductivity analysis

For B- and SP-TCOs, we considered a single layer of TCO with perpendicularly incident solar light. In order to simplify the discussion, we did not take into account any interband transitions due to light absorption. The conclusions thus apply only for materials with a band gap $E_g > 3$ eV. We used the Drude model to derive the reflectivity R and absorption coefficient α of B-TCOs as functions of the energy of the incoming light. We obtained the mean transmittance of visible light by integrating the transmittance of the solar black-body spectrum between 1.77 and 3.18 eV. The details and equations are given in Ref. [25], Secs. 1 and 2.

We used a simple Marcus model for the case of SP-TCOs [50,51]. The system in a relaxed small-polaron state can absorb a photon to reach (a) a small-polaron excited state at a neighboring site or (b) the delocalized state, where the carrier is bandlike [52]. More information on these transitions is given in Ref. [25], Sec. 3.

B. *Ab initio* computations

First-principles density functional theory (DFT) calculations have been carried out with the Vienna Ab initio simulation package (VASP) as well as with the ABINIT software [53,54]. We used the Perdew-Burke-Ernzerhof (PBE) generalized gradient approximation (GGA) [55]. A Hubbard correction U (DFT + U) has been applied on the exchange-correlation functional to enable the localization of the hole [56]. This methodology has been used in many studies and has proven to be effective [15,57,58]. We chose $U = 3.7$ eV so that the computed band gap of $LaCrO_3$ corresponds to the experimental one of 2.8 eV [14,45]. All calculations have been performed with a kinetic energy cutoff of at least 520 eV for the plane-wave basis. We used a $4 \times 4 \times 4$ Monkhorst-Pack k-point grid for the Brillouin zone integrations in the case of the primitive cell and decreased the number of grid points when the cell size increases. The cell structural relaxation processes have been realized with a convergence criterion of 0.01 eV/Å for the maximum forces, and each self-consistent field step has been done with a convergence criterion of 10^{-7} eV on the total energy. Polaron computations were performed using supercells and introducing holes (removing electrons). We checked for small-polaron formation by observing the magnetic moment on the Cr atoms as well as the Cr-O bond lengths. The magnitude of the magnetic moment on the concerned Cr atom decreases by roughly 1 μ_B (Bohr magneton) when the hole is localized, effectively going from a Cr^{3+} to a Cr^{4+} state. We confirmed the antiferromagnetic configuration observed experimentally due to the antiparallel magnetic moments of the Cr atoms [46,59].

The solid-state climbing image nudged elastic band (ss-cNEB) method has been used to compute the activation energy for small-polaron hopping [60,61]. We first interpolated the atomic positions between two neighboring small-polaron configurations of same spin orientation to obtain images along a migration path. The NEB method finds the minimum energy path between the first and the last images.

ACKNOWLEDGMENTS

G.B., G.-M.R., and G.H. acknowledge the F.R.S.-FNRS for financial support. Computational resources have been provided by the supercomputing facilities of the UCLouvain (CISM/UCL) and the Consortium des Équipements de Calcul Intensif (CÉCI), funded by the Fonds de la Recherche Scientifique de Belgique (F.R.S.-FNRS) under Grant No. 2.5020.11 and by the Walloon Region. The present research benefited from computational resources made available on the Tier-1 supercomputer of the Fédération Wallonie-Bruxelles, infrastructure funded by the Walloon Region under the Grant Agreement No. 1117545.

[1] K. Ellmer, Nat. Photon. **6**, 809 (2012).
[2] A. B. Kehoe, E. Arca, D. O. Scanlon, I. V. Shvets, and G. W. Watson, J. Phys.: Condens. Matter **28**, 125501 (2016).
[3] T. Moss, Proc. Phys. Soc. Sect. B **67**, 775 (1954).
[4] E. Burstein, Phys. Rev. **93**, 632 (1954).
[5] M. Kul, M. Zor, A. S. Aybek, S. Irmak, and E. Turan, Sol. Energy Mater. Sol. Cells **91**, 882 (2007).
[6] R. Kumaravel, K. Ramamurthi, and V. Krishnakumar, J. Phys. Chem. Solids **71**, 1545 (2010).
[7] T. Minami, Semicond. Sci. Technol. **20**, S35 (2005).
[8] G. Hautier, A. Miglio, G. Ceder, G.-M. Rignanese, and X. Gonze, Nat. Commun. **4**, 2292 (2013).
[9] L. Castañeda, Mater. Sci. Appl. **02**, 1233 (2011).
[10] J. Tate, M. Jayaraj, A. Draeseke, T. Ulbrich, A. Sleight, K. Vanaja, R. Nagarajan, J. F. Wager, and R. Hoffman, Thin Solid Films **411**, 119 (2002).
[11] K. H. Zhang, K. Xi, M. G. Blamire, and R. G. Egdell, J. Phys.: Condens. Matter **28**, 383002 (2016).
[12] P. P. Edwards, A. Porch, M. O. Jones, D. V. Morgan, and R. M. Perks, Dalton Trans., 2995 (2004).
[13] M. Dekkers, G. Rijnders, and D. H. A. Blank, Appl. Phys. Lett. **90**, 021903 (2007).
[14] K. H. Zhang, Y. Du, A. Papadogianni, O. Bierwagen, S. Sallis, L. F. Piper, M. E. Bowden, V. Shutthanandan, P. V. Sushko, and S. A. Chambers, Adv. Mater. **27**, 5191 (2015).
[15] K. H. L. Zhang, Y. Du, P. V. Sushko, M. E. Bowden, V. Shutthanandan, S. Sallis, L. F. J. Piper, and S. A. Chambers, Phys. Rev. B **91**, 155129 (2015).
[16] L. Farrell, E. Norton, C. M. Smith, D. Caffrey, I. V. Shvets, and K. Fleischer, J. Mater. Chem. C **4**, 126 (2016).
[17] E. Arca, K. Fleischer, and I. Shvets, Appl. Phys. Lett. **99**, 111910 (2011).
[18] P. L. Popa, J. Crêpellière, P. Nukala, R. Leturcq, and D. Lenoble, Appl. Mater. Today **9**, 184 (2017).
[19] J. Crêpellière, P. L. Popa, N. Bahlawane, R. Leturcq, F. Werner, S. Siebentritt, and D. Lenoble, J. Mater. Chem. C **4**, 4278 (2016).
[20] L. Farrell, K. Fleischer, D. Caffrey, D. Mullarkey, E. Norton, and I. V. Shvets, Phys. Rev. B **91**, 125202 (2015).
[21] J. B. Varley, A. Janotti, C. Franchini, and C. G. Van de Walle, Phys. Rev. B **85**, 081109(R) (2012).
[22] A. Bosman and H. Van Daal, Adv. Phys. **19**, 1 (1970).
[23] J. Bellingham, W. Phillips, and C. Adkins, J. Mater. Sci. Lett. **11**, 263 (1992).
[24] H. Peng, A. Zakutayev, S. Lany, T. R. Paudel, M. d'Avezac, P. F. Ndione, J. D. Perkins, D. S. Ginley, A. R. Nagaraja, N. H. Perry *et al.*, Adv. Funct. Mater. **23**, 5267 (2013).
[25] See Supplemental Material at http://link.aps.org/supplemental/10.1103/PhysRevMaterials.3.064602 for more information about computational details and results.
[26] K. Fleischer, E. Norton, D. Mullarkey, D. Caffrey, and I. V. Shvets, Materials **10**, 1019 (2017).
[27] D. Emin, Phys. Rev. B **48**, 13691 (1993).
[28] S. Mildner, J. Hoffmann, P. E. Blöchl, S. Techert, and C. Jooss, Phys. Rev. B **92**, 035145 (2015).
[29] J. T. Devreese, Encycl. Appl. Phys. **14**, 383 (1996).
[30] N. A. Deskins and M. Dupuis, Phys. Rev. B **75**, 195212 (2007).
[31] G. Haacke, J. Appl. Phys. **47**, 4086 (1976).
[32] R. G. Gordon, MRS Bull. **25**, 52 (2000).
[33] J. Mendez-Gamboa, R. Castro-Rodriguez, I. Perez-Quintana, R. Medina-Esquivel, and A. Martel-Arbelo, Thin Solid Films **599**, 14 (2016).
[34] D. A. Jacobs, K. R. Catchpole, F. J. Beck, and T. P. White, J. Mater. Chem. A **4**, 4490 (2016).
[35] L. Zhang, Y. Zhou, L. Guo, W. Zhao, A. Barnes, H.-T. Zhang, C. Eaton, Y. Zheng, M. Brahlek, H. F. Haneef *et al.*, Nat. Mater. **15**, 204 (2016).
[36] C. P. Liu, Y. Foo, M. Kamruzzaman, C. Y. Ho, J. A. Zapien, W. Zhu, Y. J. Li, W. Walukiewicz, and K. M. Yu, Phys. Rev. Appl. **6**, 064018 (2016).
[37] S. Calnan and A. Tiwari, Thin Solid Films **518**, 1839 (2010).
[38] K. M. Yu, M. A. Mayer, D. T. Speaks, H. He, R. Zhao, L. Hsu, S. S. Mao, E. Haller, and W. Walukiewicz, J. Appl. Phys. **111**, 123505 (2012).
[39] H. Liu, V. Avrutin, N. Izyumskaya, Ü. Özgür, and H. Morkoç, Superlattices Microstruct. **48**, 458 (2010).
[40] Z. Ma and B. He, in *Solar Cells-Thin-Film Technologies* (IntechOpen, London, 2011).
[41] R. Bernal-Correa, A. Morales-Acevedo, J. Montes-Monsalve, and A. Pulzara-Mora, J. Phys. D **49**, 125601 (2016).
[42] M. Despeisse, M. Boccard, G. Bugnon, P. Cuony, T. Söderström, G. Parascandolo, M. Stuckelberger, M. Charrière, L. Löfgren, C. Battaglia, S. Hänni, A. Billet, L. Ding, S. Nicolay, F. Sculati-Meillaud, N. Wyrsch, and C. Ballif, Proceedings of the 25th EU-PVSEC **1**, 2793 (2010).
[43] J. B. Varley, A. Miglio, V.-A. Ha, M. J. van Setten, G.-M. Rignanese, and G. Hautier, Chem. Mater. **29**, 2568 (2017).
[44] G. J. Exarhos, C. F. Windisch Jr., K. F. Ferris, and R. R. Owings, Appl. Phys. A **89**, 9 (2007).
[45] K. Maiti and D. D. Sarma, Phys. Rev. B **54**, 7816 (1996).
[46] P. V. Sushko, L. Qiao, M. Bowden, T. Varga, G. J. Exarhos, F. K. Urban III, D. Barton, and S. A. Chambers, Phys. Rev. Lett. **110**, 077401 (2013).
[47] J. Zhang, W. Li, R. Hoye, J. L. Macmanus-Driscoll, M. Budde, O. Bierwagen, L. Wang, Y. Du, M. Wahila, L. Piper *et al.*, J. Mater. Chem. C **6**, 2275 (2018).
[48] H. Chen and J. H. Harding, Phys. Rev. B **85**, 115127 (2012).
[49] W.-L. Jang, Y.-M. Lu, W.-S. Hwang, and W.-C. Chen, J. Eur. Ceram. Soc. **30**, 503 (2010).

[50] R. A. Marcus and N. Sutin, Biochimica et Biophysica Acta (BBA) - Reviews on Bioenergetics **811**, 265 (1985).
[51] R. A. Marcus, Rev. Mod. Phys. **65**, 599 (1993).
[52] L. Bjaalie, D. Ouellette, P. Moetakef, T. Cain, A. Janotti, B. Himmetoglu, S. Allen, S. Stemmer, and C. Van de Walle, Appl. Phys. Lett. **106**, 232103 (2015).
[53] X. Gonze, F. Jollet, F. A. Araujo, D. Adams, B. Amadon, T. Applencourt, C. Audouze, J.-M. Beuken, J. Bieder, A. Bokhanchuk *et al.*, Comput. Phys. Commun. **205**, 106 (2016).
[54] B. Amadon, F. Jollet, and M. Torrent, Phys. Rev. B **77**, 155104 (2008).
[55] J. P. Perdew, K. Burke, and M. Ernzerhof, Phys. Rev. Lett. **77**, 3865 (1996).
[56] P. Erhart, A. Klein, D. Åberg, and B. Sadigh, Phys. Rev. B **90**, 035204 (2014).
[57] B. Himmetoglu, A. Janotti, L. Bjaalie, and C. G. Van de Walle, Phys. Rev. B **90**, 161102(R) (2014).
[58] T. Maxisch, F. Zhou, and G. Ceder, Phys. Rev. B **73**, 104301 (2006).
[59] M. Tseggai, P. Nordblad, R. Tellgren, H. Rundlöf, G. André, and F. Bourée, J. Alloys Compd. **457**, 532 (2008).
[60] G. Henkelman, B. P. Uberuaga, and H. Jónsson, J. Chem. Phys. **113**, 9901 (2000).
[61] G. Henkelman and H. Jónsson, J. Chem. Phys. **113**, 9978 (2000).